BIOCHEMISTRY
including biophysical chemistry & molecular biology
Article

Biochemistry **2011,** *50,* 1143–1152 1143
DOI: 10.1021/bi101555y

Optimal Salt Bridge for Trp-Cage Stabilization†

D. Victoria Williams, Aimee Byrne, James Stewart, and Niels H. Andersen*

Department of Chemistry, University of Washington, Seattle, Washington 98195, United States

Received September 24, 2010; Revised Manuscript Received November 23, 2010

ABSTRACT: Gai and co-workers [Bunagan, M. R., et al. (2006) *J. Phys. Chem. B 110*, 3759−3763] reported computational design studies suggesting that a D9E mutation would stabilize the Trp-cage. Experimental studies for this mutation were reported in 2008 [Hudaky, P., et al. (2008) *Biochemistry 47*, 1007−1016]; the authors suggested that [D9E]-TC5b presented a more compact and melting resistant structure because of the "optimal distance between the two sides of the molecule". Nonetheless, the authors reported essentially the same circular dichroism (CD) melting temperature, 38 ± 0.3 °C, for TC5b and its [D9E] mutant. In this study, a more stable Trp-cage, DAYAQ WLKDG GPSSG RPPPS, was examined by nuclear magnetic resonance and CD with the following mutations: [D9E], [D9R,R16E], [R16O], [D9E,R16O], [R16K], and [D9E,R16K]. Of these, the [D9E] mutant displayed the smallest acidification-induced change in the apparent T_m. In analogy to the prior study, the CD melts of TC10b and its [D9E] mutant were, however, very similar; all of the other mutations were significantly fold destabilizing by all measures. A detailed analysis indicates that the original D9−R16 salt bridge is optimal with regard to fold cooperativity and fold stabilization. Evidence of salt bridge formation is also provided for a swapped pair, the [D9R,R16E] mutant. Model systems reveal that an ionized aspartate at the C-terminus of a helix significantly decreases intrinsic helicity, a requirement for Trp-cage fold stability. The CD evidence that was cited as supporting increased fold stability for [D9E]-TC5b at higher temperatures appears to be a reflection of increased helix stability in both the folded and unfolded states rather than a more favorable salt bridge. Our study also provides evidence of other Trp-cage stabilizing roles of the R16 side chain.

The evaluation of the effects of Coulombic interactions on protein folding remains problematic. The introduction of favorable Coulombic interactions between the termini has been shown to stabilize hairpins, but the net effect is quite small, at most a few kilojoules per mole (*1*−*3*). It has long been known (*4*−*6*) that hydrogen bonding between charged sites in proteins has a more favorable effect on folding than other H-bonding interactions. Acid−base titration studies and site mutations have uncovered 12−20 kJ/mol stabilizations associated with buried H-bonded salt bridges involving Asp−His (*7*), Asp−Arg (*8*), and Glu−Arg (*9*) side chains. A buried Asp-α-carboxylate−Arg interaction in a crambin model (*10*) has been shown to be essential for efficient folding and the formation of the correct disulfide pairing, and Asp−Arg, as well as Glu−Arg, salt bridges at dimer interfaces are required for protein kinase activation (*11*). The case for solvent-exposed Coulombic interactions (*12*) and salt bridges (*13*, *14*) is less clear; smaller but still significant effects on fold stability have been noted. As a result of desolvation issues, buried salt bridges can be replaced with hydrophobic pairings, typically with an increase in fold stability (*9*). This would not apply to exposed salt bridges and other favorable Coulombic pairings on protein surfaces. Approximately 4 kJ/mol stabilizations have been measured for favorable surface charge−charge interactions with an additional 4 kJ/mol of stabilization suggested in one case for a carboxylate−arginine H-bonding interaction (*15*). In the case of ubiquitin (*16*), 4−7 kJ/mol effects on fold stability can result from charge reversals on the surface. Favorable carboxylate−Lys interactions have been implicated in the stability of a 39-residue minimized fold motif (*17*). Charged side chain interactions can even alter the potential energies of unfolded states; Cho and Raleigh (*18*) have reported a case of an 8 kJ/mol stability increase in a truncated protein as a result of removal of a favorable Coulombic effect in the unfolded state. As a result, questions concerning the effects of charge pairing and salt bridging at surface sites in proteins remain.

The Trp-cage fold (*19*), with a length of 18−25 residues (*20*, *21*), is the smallest fold that can be viewed as a globular protein. It consists of an N-terminal α-helix, a short 3_{10}-helix, a C-terminal poly-ProII helix, and a hydrophobic core with a buried Trp indole ring at its center. As a result of its small size, the Trp-cage became a target of molecular dynamics simulated folding (*22*, *23*) as soon as the structure was published; subsequent computational studies (*24*−*39*) have established it as a protein folding paradigm (*40*, *41*). Trp-cage species have also proven to be useful for quantitating fold stability effects of side chain interactions and mutations that influence the intrinsic stability of secondary structure features (*20*, *21*, *42*). A solvent-exposed Asp−Arg salt bridge (D9−R16) has been reported to provide 4.7 ± 1.3 kJ/mol of fold stabilization in Trp-cage species (*21*). The formation of this Asp−Arg salt bridge is viewed as an important driver in the folding simulations, typically as a fold facilitating interaction (*23*, *24*); however, in some folding simulations, it appears as a stabilizing feature in kinetic traps (*27*, *31*, *32*, *39*).

Although the original Trp-cage construct (TC5b, NLYIQ WLKDG GPSSG RPPPS) (*19*) is only marginally stable with

†The authors acknowledge the National Institutes of Health for financial support (GM059658) of this work.

*To whom correspondence should be addressed. E-mail: andersen@chem.washington.edu. Telephone: (206) 543-7099. Fax: (206) 685-8665.

Published on Web 01/11/2011

a melting temperature, T_m, of 42 °C (ΔG_U^{280} = 9 kJ/mol), it continues to be the subject of both MD folding simulations (*43*−*46*) and experimental studies (*41*, *47*−*51*) even though more stable constructs with Asp as the helix N-cap and L-Ala (*20*, *21*, *52*) and D-Ala (*53*) substitutions have been reported. Recent reports for TC5b have given comparable T_m values: 43.7 ± 1.8 °C from a combined analysis of calorimetry and CD data (*54*) and 41 ± 2 °C from an analysis of CD melts over a range of urea denaturant concentrations (*51*). Recent computational estimates (*55*) of the thermodynamic stability of TC5b [T_m = 48 °C (*55*)] are also approaching the experimental values rather than yielding fold stabilities far in excess of that observed. In 2006, Gai and co-workers (*47*) reported computational design studies suggesting that D9E and P12W mutations would stabilize the Trp-cage; their experimental studies confirmed the stabilizing effect of the P12W mutation on TC5b. A later report (*56*) indicated that the D9E mutation was also stabilizing. The primary evidence for this conclusion was the retention, in the [D9E] mutant of TC5b, of both more long-range NOEs and a more helical CD spectrum at higher temperatures. The authors suggested that [D9E]-TC5b presents a more compact and melting resistant structure because of the "optimal distance between the two sides of the molecule". Nonetheless, the authors reported essentially the same CD melting temperature, 38 ± 0.3 °C, for TC5b and its [D9E] mutant at pH ~6.6, implying that the higher-temperature nuclear magnetic resonance (NMR) ensembles are based on constraints obtained for a ~60:40 mixture of folded and unfolded species. Also, the CD melt reported for the [D9E] mutant was more gradual, which is often equated with less cooperativity of folding. In our view, the question of Trp-cage salt bridge optimization needed to be re-examined; we opted for a mutational study of the TC10b Trp-cage (DAYAQ WLKDG GPSSG RPPPS; T_m = 56 °C; ΔG_U^{280} = 12 kJ/mol) (*20*, *21*). The studies reported herein indicate that the original D9−R16 salt bridge was, indeed, already optimized with regard to folding cooperativity. The CD evidence that was cited as supporting increased fold stability for the D9E mutant of TC5b at higher temperatures appears to be a reflection of increased helix stability in both the folded and unfolded state rather than a more favorable salt bridge. This study also provides evidence of other cage stabilizing roles of the R16 side chain.

MATERIALS AND METHODS

Peptide Synthesis and Purification. Linear peptides were synthesized on an Applied Biosystems 433A synthesizer employing standard Fmoc (9-fluorenylmethoxycarbonyl) solid-phase peptide synthesis methods and purified using RP-HPLC, using C_{18} and/or C_8 stationary phases and a water (0.1% trifluoroacetic acid)/acetonitrile (0.085% trifluoroacetic acid) gradient as previously described (*21*). The resins used for the synthesis were Wang resins preloaded with the C-terminal amino acid. Peptides were cleaved from the resin using a 95:2.5:2.5 trifluoroacetic acid/triisopropylsilane/water mixture. The sequences of all peptides were confirmed by the molecular ions observed using Bruker Esquire ion trap mass spectrometry.

NMR Spectroscopy. Samples for two-dimensional (2D) NMR spectral studies consisted of ~1.5 mM peptide in 50 mM phosphate buffer (pH 7) and 10% D_2O, with DSS[1] as an internal chemical shift reference. NMR experiments were conducted at 500 or 750 MHz on Bruker DRX and AV spectrometers. Full ^{1}H spectral assignments were made by using a combination of 2D NOESY and TOCSY experiments. NMR structure ensembles were generated in the manner previously described (*19*, *21*); the details appear in the Supporting Information. The HN and Hα chemical shift deviations (CSDs) were calculated using the then current CSDb algorithm (*2*) and were found to be consistent with all other Trp-cage constructs: large characteristic CSDs include G11 Hα2 (3.5−3.7 ppm upfield) and P18 Hβ3 and Hα (~2.15 and 2.3 ppm upfield, respectively). In NMR melts, plots of these large CSDs, as well as smaller but also diagnostic CSDs at L7 Hα and P19 H$\delta\delta'$, versus temperature are used to derive fold populations as previously described (*21*, *53*). Briefly, CSDs are derived from spectra recorded at 280−330 K (in 10 K increments). The CSDs observed for TC10b at 280 K are equated with a χ_F value of 0.994. Thus, the value for an analogue at any temperature corresponds to 0.994 ($CSD_{obs}/CSD_{TC10b}^{280K}$). This assumes that folded state structuring shifts are not temperature-dependent and are identical for all species adopting the Trp-cage folding motif. Whenever possible, we employ the sum of the CSDs noted above for χ_F calculations. For some species, the G11 Hα2 signal displays exchange broadening to the extent that the peak disappears from the 2D spectra; in such cases, we use the sum over the available ring current shifts.

Recent studies (unreported to date) have revealed that very large ring current effects do decrease slightly on warming even when χ_F does not increase significantly. A 1% loss per 10 °C in the large ring current shifts has been observed for hyperstable species that are demonstrably 99% folded by CD throughout the 5−35 °C range. No correction for this effect was applied. Small differences in CSDs could result from quite subtle changes in Trp-cage fold geometry. The resulting errors in χ_F are on the order of ±0.02 throughout the range examined. These errors are unacceptable for χ_F estimates greater than 0.92; as a result, we do not rely on $\Delta\Delta G$ values for comparisons, including species with χ_F values of > 0.92 for our conclusions. The ΔG_U and $\Delta\Delta G$ values are calculated on the basis of the derived χ_F values as $\Delta G_U = RT \ln[\chi_F/(1 - \chi_F)]$. In the case of TC10b, the ΔG_U value (ΔG_U^{298} = 5.56 ± 0.11 kJ/mol) has been validated by a full thermodynamic fit (*21*). At 300 K, the χ_F values derived from CSDs for the mutants examined are in the range where ΔG errors are equal to or less than 0.36 kJ/mol.

Circular Dichroism Spectroscopy. Stock solutions of approximately 200 μM peptide were prepared using 20 mM aqueous phosphate buffer (pH 7.0). Accurate concentrations were determined by UV spectroscopy assuming the standard molar absorptivities for the Trp and Tyr residues present. The samples were then diluted appropriately with buffer to yield ~30 μM peptide solutions. Spectra, and the corresponding buffer blanks, were recorded on a Jasco J720 spectropolarimeter using 0.10 cm path length cells over a UV range of 190−270 nm with 8−12 scans averaged for each spectrum with ellipticities reported in deg-cm^2/residue-decimole units. Temperatures ranged from 5 to 90 °C in 5−10 °C increments. The final spectra for each temperature were obtained as differences between the sample and buffer blank, both set to zero at 260 nm, after the FFT filter in the Jasco spectra processing software had been employed.

The folded fraction (χ_F) was determined by defining the temperature-dependent CD signal of the unfolded and folded states and assuming a linear χ_F relationship for signals between

[1]Abbreviations: TFA, trifluoroacetic acid; DSS, 2,2-dimethyl-2-silapentane-5-sulfonate; CSD, chemical shift deviation. The standard one- and three-letter symbols for amino acids are employed with O used for ornithine (Orn).

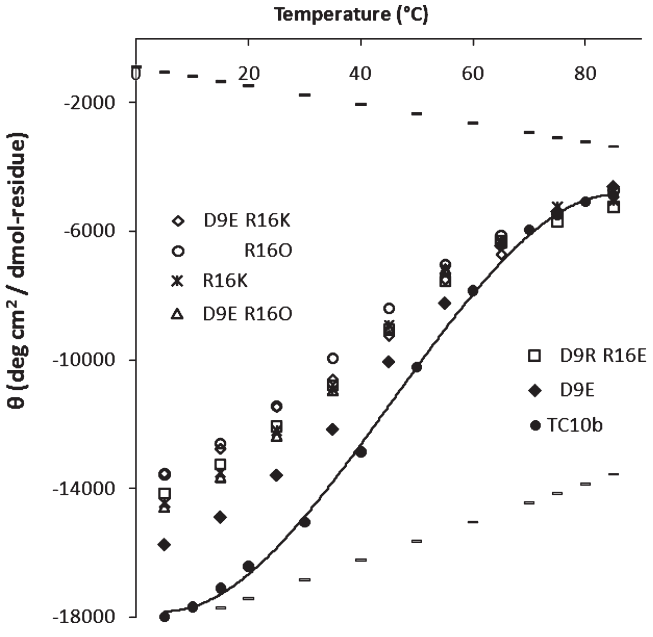

FIGURE 1: CD melts (raw ellipticity values vs T) of TC10b and its [D9E], [R16O], [R16K], [D9E,R16O], [D9E,R16K], and [D9R, R16E] mutants. The points for TC10b are fitted to a third-order polynomial to provide a line to guide the eye. The unfolded and folded state baselines for TC10b are also shown in the plot (---). The corresponding plots of data for pH 2.5 appear in Figure S1 of the Supporting Information.

the two lines. The CD spectrum of the unfolded state is expected, as long as the constructs contain a single Tyr and Trp residue, to be sequence-independent and has been previously determined for several Trp-cage constructs in >6.5 M Gdm^+Cl^- (*21*, *57*). For our study, [R16K]-TC10b was examined under these denaturing conditions, affording a coil value for $[\theta]_{222}$ of $-560 - 25T$(°C); this addition brings the average Trp-cage coil baseline ($n = 5$) to a $[\theta]_{222}$ of $-750 - 27T$(°C). This baseline was employed for Figure 5 and for deriving the ΔG values in Table 2. The unfolded baseline for wild-type (WT) TC10b [$[\theta]_{222} = -900 - 29T$(°C)] from the thermodynamic fit (*21*) was retained for Figure 1.

In previous studies of Trp-cage species in this laboratory, folded baselines derived from the CD melts corresponded to a 0.30−0.34% loss of signal per degree Celsius: $[\theta]_F = [\theta]_{F,0°C} - 0.0032[\theta]_{F,0°C}T$(°C). This value has been confirmed for hyperstable Trp-cage mutants [$T_m \geq 83$ °C (*53*)] that display a folded native state population greater than 98% over the 5−35 °C temperature range. This was, in the absence of evidence to the contrary, assumed for our constructs. Values of $[\theta]_{F,0°C}$ were calculated using the same temperature-dependent slope with the 100% folded values at 7 °C at both pH 7 and 2.5 derived as $[\theta]_{obs}/\chi_F$(NMR). The $[\theta]_{F,0°C}$ values used to generate the melting curves in Figure 5 were: −18350° (−16700° at pH 2.5) for TC10b, −16480° (−18300° at pH 2.5) for [D9E], −14700° for [D9E,R16K], −15200° (−13650° at pH 2.5) for [D9R,R16E], −15820° for [R16K], and −15600° (−12700° at pH 2.5) for [R16O].

There is one other report of Trp-cage CD baselines; Streicher and Makhatadze (*54*) arrived at $[\theta]_{222}{}^N = [-18000 + 44T(°C)]°$ and $[\theta]_{222}{}^U = [-4740 - 7.4T(°C)]°$ for TC5b. The former corresponds to a 0.24%, rather than 0.32%, loss of signal per degree Celsius for the folded state. Even though the unfolded baseline of Streicher and Makhatadze is significantly different than our 7 M GdmCl baseline for TC5b ($-661 - 29.6T$), in no case would the use of this alternative unfolded baseline and the smaller $[\theta]_{222}$ gradient for the folded state change a reported T_m value by more than 2 °C.

RESULTS

An R16K mutation of the D9−R16 unit has already been reported (*21*) for TC10b, and D9N and R16Nva (norvaline, the des-guanidino analogue of Arg) mutations were reported for the corresponding sequence with an N-terminal Asn. Additional data for the R16K mutant are included here. As anticipated, on the basis of a fold stabilizing role for a D9−R16 salt bridge, the destabilization of TC10b ($\Delta T_m = -17$ °C) observed upon protonation of the carboxylates (pH 2.5 vs pH 7) disappeared for the (D1N,R16Nva) double mutation. The R16K mutation was destabilizing, but the stability loss was smaller than the factor associated with the D9−R16 interaction, suggesting that the D−K charge−charge interaction does provide some fold stabilization. This, together with our concerns about the conclusions reported by Perczel and co-workers (*56*), prompted us to examine additional mutations of TC10b to probe the chain length dependence and directionality of this Coulombic effect. The [D9E], [R16O], [D9E,R16O], [D9E,R16K], and [D9R,R16E] mutants were prepared. The CD melts for the newly synthesized species at pH 7 are compared to the "wild type" in Figure 1.

It was immediately apparent that WT TC10b displayed the largest $[\theta]_{222}$ values and the sharpest unfolding transition in the CD melt. All of the mutants exhibited smaller ellipticities at the low-temperature limit, but the [D9E] mutant had, in agreement with reported data for this mutation of TC5b, a larger negative ellipticity at higher temperatures. All of the mutants exhibited less cooperative melts and less evidence of approaching a 100% folded plateau at the low temperature. The three species that were also examined at pH 2.5 (Figure S1 of the Supporting Information) exhibited clear evidence of fold destabilization as a result of carboxylate protonation; of these, the [D9E] mutant displayed the smallest acidification-induced change in the apparent T_m. However, these changes cannot be assigned exclusively to disruption of the residue 9−residue 16 side chain interaction (vide infra). For an initial estimate of T_m values (Table 1), we assumed that the CD spectrum for the fully folded Trp-cage state at the two pH values is not changed by these mutations. Because this assumption is not necessarily valid, we also examined chemical shift measures of folding.

The Trp-cage fold displays consistent dramatic upfield shifts because of ring current effects. The sum of the L7 Hα, P18 Hα,β3, and P19 Hδ2,δ3 CSDs has been established as a measure of the extent of cage formation (*21*); when available, the CSD of the upfield G11 Hα is also included in this measure of the extent of folding. The diastereotopic chemical shift difference observed for the Gly11 CH_2 ($\Delta\delta$G11) is another useful diagnostic. In prior studies (*1*, *19*, *21*, *42*), partial melting as well as all destabilizing mutations decreased $\Delta\delta$G11, reflecting increases in the contribution of the unfolded state. However, changes in $\Delta\delta$G11 could also reflect changes in the geometry of the loop connecting the helix to the docked triproline unit or the fluxionality of the fold.

The entries in Table 1 appear in order of decreasing values for the chemical shift changes that are diagnostic of cage formation. This also corresponds to the ordering based on the apparent melting temperatures. The ranking based on $\Delta\delta$G11 has one

Table 1: NMR and CD Measures of Fold Stability for TC10b and Mutants at 280 K[a]

peptide	sequence	∑CSDs (with 11α2)	Δδ G11	T_M CD (°C) vs 10b reference
TC10b	DAYAQWLKDGGPSSGRPPPS	6.534 (10.028)	2.486	56
TC10b at pH 2.5		5.80 (8.67)	1.700	39
[D9E]	DAYAQWLK**E**GGPSSGRPPPS	6.436 (9.725)	2.203	52
[D9E] at pH 2.5		5.61	not available	44
[D9E,R16K]	DAYAQWLK**E**GGPSSG**K**PPPS	6.236 (9.399)	2.067	47
[D9R,R16E]	DAYAQWLK**R**GGPSSG**E**PPPS	6.204 (9.059)	**1.648**	47
[D9R,R16E] at pH 2.5		4.81 (7.33)	**1.623**	17
[R16K]	DAYAQWLKDGGPSSG**K**PPPS	6.059 (9.128)	1.976	46
[D9E,R16O]	DAYAQWLK**E**GGPSSG**O**PPPS	5.972 (9.038)	1.989	46
[R16O]	DAYAQWLKDGGPSSG**O**PPPS	5.732 (8.684)	1.872	42
[R16O] at pH 2.5		5.13 (7.71)	1.440	21

[a]The CD melting temperatures reported here assume that the folded and unfolded baselines for TC10b (at each pH) apply for all of the mutants.

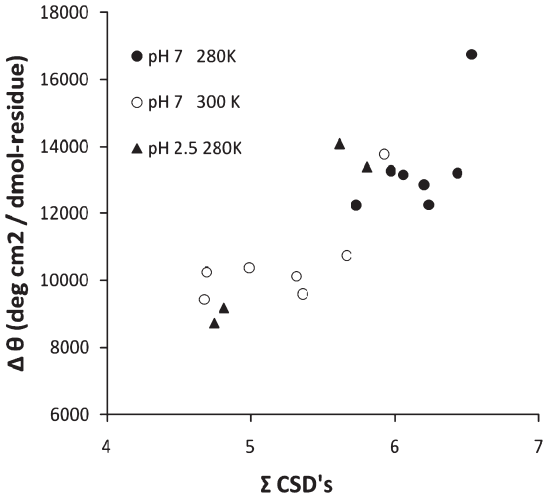

FIGURE 2: Correlation between ∑CSDs and $-([\theta]_{obv} - [\theta]_U)$ values: 280 K at pH 7 (●) and pH 2.5 (▲) and 300 K (○). Extrapolation of the best fit line to $([\theta]_{obv} - [\theta]_U) = 0$ yields a ∑CSDs value of 1.6, suggesting some residual structuring is present in the unfolded state.

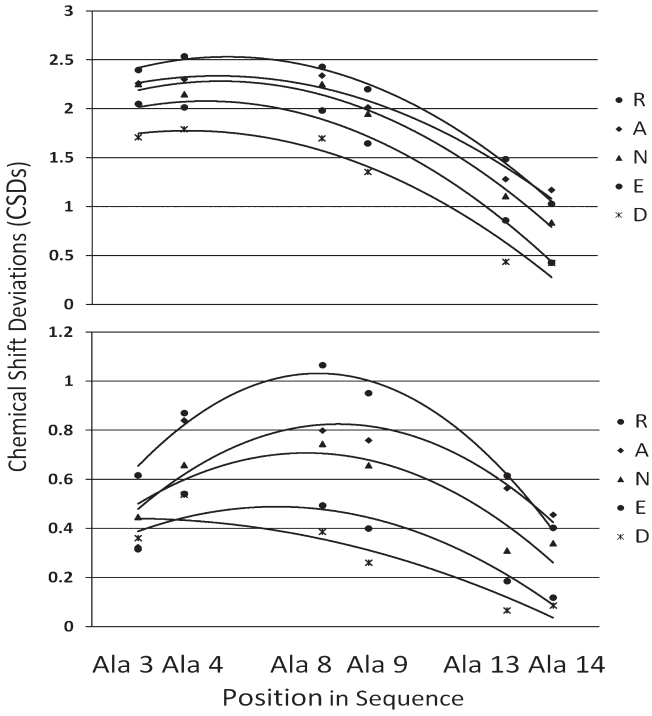

FIGURE 3: Sequence plot of the Ala $^{13}C{=}O$ CSDs along the sequence of Ac-KAAAAKAAAAKAAAAXGY-NH_2 (top) and the desacetyl species (bottom) at pH 7. In the central repeat, a CSD of 3.5 ppm corresponds to 100% helicity. For the less stable desacetyl peptides, the relative helicities are in the same order with all values decreased; however, the differences (in $\Delta\Delta G$ units) are exaggerated in the less stable desacetyl series of peptides.

notable outlier; the [D9R,R16E] double mutant that reverses the directionality of the potential salt bridge has the smallest Δδ G11 value at pH 7, and this value does not decrease upon acidification, even though other measures of folding indicate decreased fold stability at pH 2.5. There is an acceptable correlation (R^2 = 0.72) between the ∑CSDs measure of folding and the amplitude of the CD spectrum, as gauged by the $-([\theta]_{obv} - [\theta]_U)$ values at 222 nm (Figure 2). The effects of acidification and partial melting are also included in Figure 2.

One anticipated effect of acidification on fold stability is constant in this series. Asp^- has a larger N-capping constant, N_{cap} (12), than Asp^0 (4.8) on the basis of a recent recalibration (*58*) of the extended Lifson−Roig helix−coil (*59*) parameters. As a result, protonation of the N-terminal Asp destabilizes the N-terminal helix and thus the Trp-cage fold. This effect would be expected to be a constant context effect throughout the series examined herein. The $\Delta\Delta G_F$ increment for N-terminal Asp protonation in model helices is ∼2 kJ/mol.

Because residue 9 is the C-terminus of this α-helix, substitutions at D9 (and ionization state changes at this site) could also influence fold stability by affecting intrinsic helix stability. The effects of substitutions at the C-terminal helix site can be modeled in a peptide helix, Ac-KAAAAKAAAAKAAAAXGY-NH_2, by varying the X site residue (X = R, A, N, E, or D). Asn was used as a surrogate for Asp^0. The CSDs of the $^{13}C{=}O$ units (*60*, *61*) of the underlined alanine sites were used to monitor helicity changes (Figure 3).

The data in Figure 3 show that an Asp → Glu mutation at the C-terminus of a peptide helix results in a significant increase in helicity at pH 7. This effect should apply to both the folded and unfolded state of Trp-cage sequences with this mutation. Helicity $\Delta\Delta G_F$ values for the acetylated species, derived from the CSDs observed in the central repeat (*60*), were −0.40 for R^+, 0.0 (the reference) for A, 0.20 for N, 0.97 for E^-, and 1.73 kJ/mol for D^-. These can serve as an estimate of the changes in Trp-cage stabilities that might be expected from effects of the D9 mutation on helix stability. On this basis, protonation of D9 (modeled as the D → N change at pH 7) is predicted to be significantly fold-destabilizing. The less stable desacetyl species presents

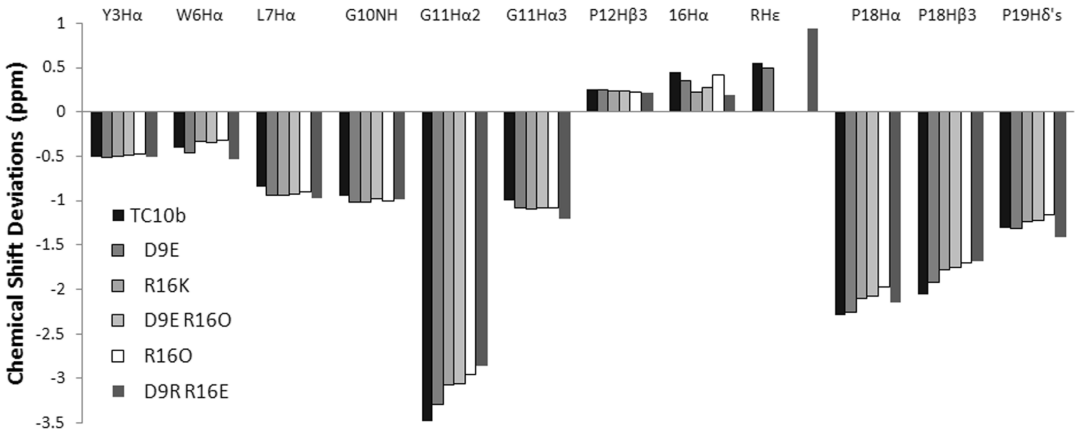

FIGURE 4: Chemical shift deviation comparisons for TC10b and mutants with mutations at D9 and/or R16. All CSDs were measured at pH 7 and 280 K. The P19 Hδ entry is the sum of the CSDs for the two Hδ resonances.

fractional helicities similar to those observed for Trp-cage sequences truncated to prevent cage formation. In the desacetyl system, $\Delta\Delta G_F(D\rightarrow N) = 1.8$ kJ/mol, essentially the same value as in the acetylated helices. A D9E mutation is thus expected to be fold stabilizing and to effect increased helicity in the unfolded state. Protonation effects for the [D9E] mutants would be expected to be smaller because the charge is farther from the helix macrodipole when the side chain is longer.

There have been a number of examples in which salt bridge stabilization remains for residue swaps [for both D−R and E−R interactions, examples appear in protein kinase activation studies (*11*)]. Such reports prompted us to examine a [D9R, R16E] mutation. This residue swap also serves as an additional probe of potential helix C-termination effects. In this case, an Arg^+ side chain at the helix C-terminus should be helix stabilizing at all pH values examined. Key CSD comparisons between TC10b and the current set of analogues appear in Figure 4. While the structuring chemical shifts at essentially all proton sites of the other TC10b mutants were uniformly concordant with those of the WT, indicating the formation of essentially the same fold geometry, the [D9R,R16E] mutant presented a number of changes.

Of particular note, the downfield shifts at P12 Hβ3 and R16 Hα indicate that these two protons are quite close to the indole ring plane in a manner independent of amino acid substitutions at residues 9 and 16: the geometry of the loop and 3_{10}-helix connecting the α-helix to the tri-Pro unit appears to be the same. These positive CSDs appear to reflect the same order of fold stability as the negative ring currents shifts at G11 Hα2 and P18 Hα,β3. The most notable changes associated with reversing the positions of the Glu and Arg units are a further downfield shift for RHε, increased negative CSDs at W6Hα as well as P19 CδH_2, and, as previously noted, a distinctly different CSD ratio for G11 Hα2 and Hα3. While the change in G11 CH_2 shifts could represent either a repositioning of the indole ring or a change in the backbone geometry in the G10−P12 loop region, these seemed to be ruled out by the typical P12 Hβ3 and R16 Hα CSDs. Because both of these species were more than 93% folded at 280 K (vide infra), higher-precision NOESY data were collected for the calculation of NMR structure ensembles. Representative members of the ensembles appear in Figure 6 (vide infra) with the complete constraints, ensembles, and statistics appearing in the Supporting Information.

DISCUSSION

Do Salt Bridge Alterations Change the Trp-Cage Structure?. Perczel and co-workers (*56*) reported that a [D9E] mutation in the marginally stable TC5b Trp-cage results in a "more compact and more thermoresistant" structure and presented NMR structure ensembles for TC5b and its [D9E] mutant at both 282 and 300 K. Even in the NMR ensembles generated on the basis of the lower-temperature NOE data, TC5b and [D9E]-TC5b did not exhibit backbone overlap over the span of residues 10−19. The NMR ensembles generated for the mutant were based on a much larger number of NOE distance restraints (324, of which 210 were inter-residue). Although the key CSDs associated with ring current effects were very similar, there were some differences noted for the NOEs; e.g., Hudáky et al. reported that the [D9E] mutant lacked NOE connectivities between the Y3 side chain and P19 sites. These through-space interactions were, however, observed for the D9E mutant of TC10b; in fact, they were observed for all of the new analogues prepared in this study. In this study, the numbers of long-range NOE constraints [residue i to $i + n$ sites ($n > 3$)] employed in the NMR structure elucidations were 40 and 55 for the [D9E] and [D9R,R16E] mutants, respectively.

Ring current calculations on structures generated during MD runs (*62*) starting from our published TC5b structure have revealed that root-mean-square deviations (rmsds) for backbone residue 3−19 within 0.9 Å of the starting structure are required for rationalization of the ring current CSDs observed for Trp-cage species (*21*). The observation that all of the mutants examined in this study reproduce (Figure 4) the key CSDs of the Trp cage, including the upfield shifts at P12 Hβ3 and R16 Hα thus implies structures within a 1 Å backbone rmsd of the standard Trp-cage conformation. In Barua et al. (*21*), we also indicated, without presenting the details, that as few as 52 medium- and long-range constraints are sufficient to generate an ensemble within a 0.63 ± 0.17 Å backbone rmsd of our published TC5b structure. In the Supporting Information, we demonstrate that a limited set of NOEs also serves to generate TC10b structures that predict all of the ring current shifts. Although high-precision NOESYs for a structure elucidation were not obtained for all of the new analogues, a survey of the NOESY data collected during the course of spectral assignment revealed that all of the new species in this report displayed a common set of 77 NOEs (of which 35 provided long-range constraints as defined above); this set of NOEs provides an NMR ensemble with an intraensemble

0.82 ± 0.33 Å rmsd for backbone residues 3−19, and within 0.90 ± 0.39 Å of a typical member of the published TC10b ensemble generated with the full set (186) of NOE constraints (of which 32 were long-range). Including one additional NOE constraint, between methylene hydrogens of residues 9 and 14, which was present for TC10b and its [D9E] and [D9R,R16E] mutants, greatly improved convergence (intraensemble rmsd of 0.58 ± 0.19 Å, nearly comparable to the value obtained with the full set of TC10b constraints, 0.41 ± 0.14 Å) and provides full agreement with the literature structure of TC10b. As a result, we conclude that salt bridge mutations of TC10b do not alter the cage conformation in an appreciable way. NOESY-based structure elucidations were also viewed as inappropriate for mutants and conditions under which the cage is < 75% folded: under such conditions, the accuracy of medium- and long-range distance constraints derived from exchange-averaged NOE intensities will be compromised, and some of the short-range constraints predominantly reflect the coil state. This combination often results in either a larger deviation between the distance constraints and distances in the structure ensemble or false convergence to a compromise structure. NMR structures were derived for the [D9R,R16E] and [D9E] mutants, among the most folded mutants examined, in an attempt to determine how these side chains and P19 orient relative to the indole ring (vide infra).

All of the TC10b mutants examined in this study exhibited additional TOCSY and NOESY peaks due to species with *cis* Xaa−Pro linkages that are not in rapid equilibrium with the all-*trans* species that folds to the Trp-cage conformation (Figure S2 of the Supporting Information); these increase in intensity on warming and acidification. Minor isomer peaks were totally absent in the spectra recorded for TC10b. This observation stands as irrefutable evidence that the Trp-cage fold is significantly destabilized for all of the mutations examined.

On the basis of exchange broadening effects, cage folding dynamics appear to be similar to those of other constructs with comparable T_m values. The highly shifted G11 Hα2 signal typically broadens into the base plane by 300 or 310 K and, in the case of the D9E mutant, is absent at pH 2.5 even at 280 K. The two exceptions to these generalities were the [D9R,R16E] and [R16O] mutants, which provided 2D spectra with G11 Hα2−Hα3 cross-peaks at all temperatures even at pH 2.5. This was particularly surprising for [R16O], the least stable of the mutants, and may indicate faster folding dynamics with this short side chain at the site of residue 16.

Rationalizing the Melting Behavior of [*D9E*] *and Other Mutated Trp-Cages*. As in the case of TC5b, a [D9E] mutation of the more stable TC10b fold showed little change in the CD melting temperature. If we use the steepness of the melt (measured, for example, as $\Delta[\theta]_{222}/\Delta T$ near the melt midpoint) as a measure of cooperativity, [D9E]-TC10b and the other mutants appear to display some loss of melting cooperativity (Figure 1). This measure, however, could be inaccurate if the 100% folded $[\theta]_{222}$ values for the different analogues differ significantly. As a result, we opted to convert the CD melts to χ_U versus T plots by estimating the 100% folded $[\theta]_{222}$ values at 280 K for each species as $[\theta]_{obs}/\chi_F$, with the χ_F value derived from NMR fold measures as $0.994(\sum CSD_{obs}/\sum CSD_{TC10b})$: amide exchange protection indicates that TC10b is 99.4% folded under these conditions. The resulting melts appear in Figure 5.

The differences in apparent cooperativity are significantly reduced after this calibration, but some distinction remains. TC10b and its [D9E] mutant have quite similar melts at both

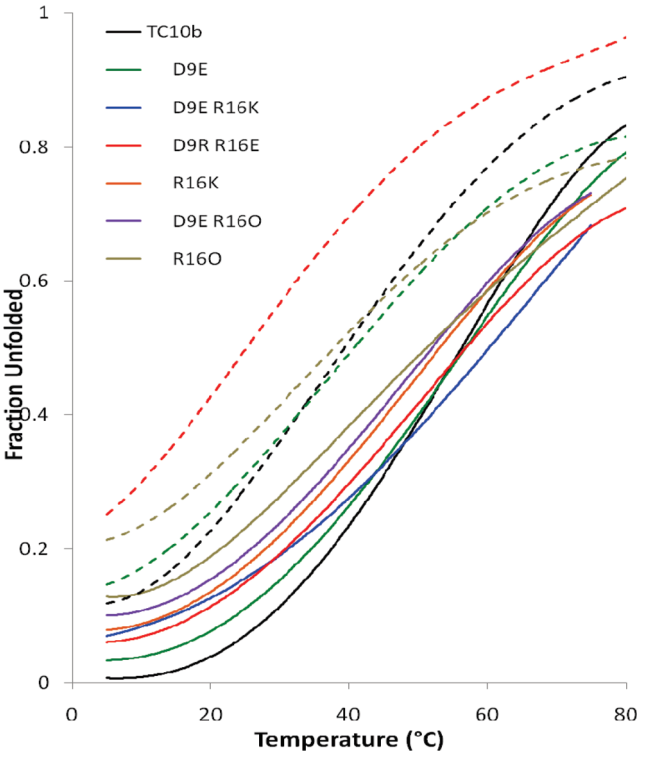

FIGURE 5: CD melts as χ_U vs T plots. Solid lines are for pH 7 data and dashed lines for pH 2.5 data. To show all of the mutants in a single figure, the data are shown as third-order polynomial fits. This polynomial fit provides an accurate location of the experimental points to guide the eye. A common unfolded baseline [$[\theta]_{222} = -750 - 27T(°C)$] was employed for all mutants; the folded baselines are given in Materials and Methods. All raw data points, as well as sigmoidal curve fits for four species, appear in the figures in the Supporting Information. The sigmoidal fits assume no helicity signal for the unfolded state and represent the expectations for melting with a strict two-state (folded−unfolded) equilibrium.

pH values examined. Using $\Delta\chi_U/\Delta T$ in the nearly linear portion of the plots as the measure of cooperativity, the [D9E] and [D9R, R16E] mutants melt somewhat less cooperatively than TC10b and the other mutants display distinctly less cooperative melting. All of the salt bridge mutants appear to retain more negative $[\theta]_{222}$ values at the higher temperatures than what would be expected on the basis of the extent of folding at the low-temperature limit or their respective T_m values; these deviations are larger for the species with a D9E or D9R mutation. This is apparent in attempts to fit the CD melting curves to the sigmoidal curve form expected for a two-state equilibrium (see the Supporting Information).

The CD minimum at 222 nm observed for Trp-cage species is predominantly due to the coupled n → π* transition of amides in the α-helix. Tyr and Trp side chain chromophores also contribute; the larger $-[\theta]_{222}$ values (21900° vs 18350° for TC10b) for Trp-cage species with D-Ala residues replacing G10 and G15 (*53*) likely reflect the further restriction of χ values for the aromatic residues in this more stable Trp-cage species. Nonetheless, it appears prudent to also consider the implications of viewing the χ_F values from Figure 5 as helicity rather than global folding measures. If there is residual helicity in the unfolded state, this would be reflected by a failure to display complete CD melting. Peptide helices generally display less cooperative CD melting "curves" than helical proteins, with a more gradual, nearly linear, loss of fractional helicity on warming. On the basis of the data presented for model helices (Figure 3), which indicate that

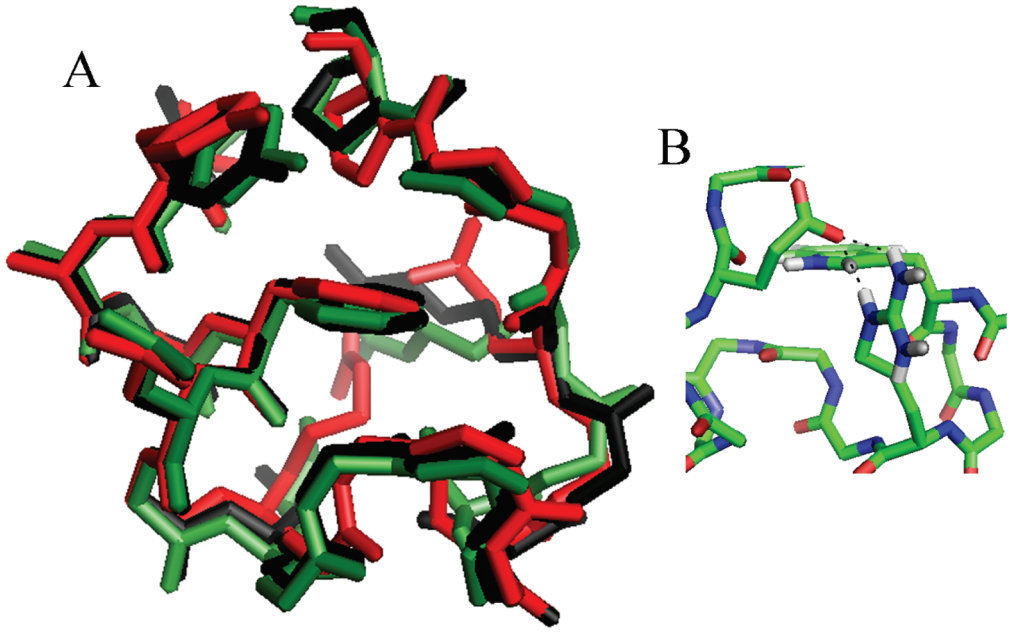

FIGURE 6: Comparison of the salt bridge mutant structures to the prior TC10b NMR ensemble. Representative structures from each ensemble are shown in panel A with the residue 2−19 backbone and the heavy atoms of residues 3, 6, 12, 16, 18, and 19: TC10b (black), [D9E] (green), and [D9R, R16E] (red). (B) R9−E16 salt bridge geometry that is frequently observed in the ensemble.

aspartate is the least favorable helix C-terminus, any of the substitutions at this site should enhance helicity, particularly in the unfolded state. Residual $-[\theta]_{222}$ values at the higher temperatures could reflect the CD contribution of helical species lacking the full cage structure. Because we view the NMR measures as the more accurate measures of cage fold populations, the remaining discussion will rely largely on NMR studies.

Trp-Cage NMR Structure Comparisons: D9−R16 Salt Bridge versus E9−R16 and R9−E16 Salt Bridges and Effects of the Glu−Arg Swap. The NOESY data sets for [D9E]- and [D9R,R16E]-TC10b provided a sufficiently rich web of NOE constraints to define their Trp-cage residue 3−19 backbone conformations to within intraresidue rmsds of < 0.3 Å (further details appear in the Supporting Information). As a result, a representative structure close to each mean can be used to represent these structures. These representative structures are superimposed on the TC10b structure in Figure 6. The [D9E] mutant structure lies within the TC10b ensemble and, like the TC10b structure, places the R16 side chain wrapping around the backside of the Trp indole ring. This function, providing burial of the Trp residue, cannot be filled by the shorter E16 side chain. This would be expected to be a fold stabilizing effect of R16 that is unrelated to salt bridge effects. π-Cation effects, an alternative source of stabilization associated with R16, appear highly unlikely because a favorable Arg−Trp π-cation effect would require placing the planar guanidinium unit (as a π-cation) over the electron-rich face of the indole ring: the TC10b and [D9E]-TC10b structures place the guanidino group of Arg in the electron-poor nodal plane rather than in the π-cloud of the indole.

The TC10b and [D9E]-TC10b structures do not provide evidence of an H-bonded Xaa9−R16 salt bridge. This could reflect the lack of definable side chain−side chain NOEs, but in the case of [D9E]-TC10b, the addition of distance constraints that would enforce a tighter salt bridge interaction introduces greater violations for NOE-based distance constraints. We have previously reported (*21*) that TC10b structures can be generated with an H-bonded salt bridge.

In the case of the [D9R,R16E] mutant, there appear to be some structural differences. (1) Even though the residue 3−19 backbone rmsd is more converged (0.17 ± 0.09 Å) in the NMR ensemble, it lies outside of the limits for the TC10b ensemble ($\langle$rmsd$\rangle = 0.63$ Å vs the TC10b representative). (2) A significant cluster of structures displays a tighter salt bridge geometry (see Figure 6B). (3) P19 and the indole ring are in closer contact. The displacement of the P19 unit closer to the indole ring is consistent with the observation of slightly larger upfield ring current shifts for P19 H$\delta\delta'$ and also alters the G11 Hα2,3 ring current prediction toward the $\Delta\delta$G11 observed for the [D9R,R16E] analogue. The [D9R,R16E] analogue ensemble also provides an explanation for the downfield shift of R9 Hε (Figure 4). This proton appears nearly in the deshielding, nodal plane of the indole ring. An H-bond to the E16 carboxylate (Figure 6B) would also result in deshielding.

Efforts To Evaluate the ΔG_U Contributions of Alternate Salt Bridge Pairings to Cage Formation. For salt-bridged systems, there are two potential sources of $\Delta\Delta G$ information, changes in fold population associated with each mutation ($m\Delta\Delta G_U$) and the effect of acidification [$\Delta\Delta G_U$(pH)]. However, there are complicating factors in the analysis of each of these $\Delta\Delta G$ values in our case. Acidification alters a number of features that could affect structure stability. As previously noted, the effects of protonation of the helix-N-capping Asp (and the C-terminal Ser-CO_2^-) are constant throughout the series, but the effects of protonating the Glu or Asp at the C-terminus of the α-helix are not. Protonation of Asp1 decreases the Trp-cage fold population by its effect on the intrinsic helicity of the N-terminal helix. The effect could be greater for CD measures of folding because removal of the N-cap would increase terminal fraying and decrease $[\theta]_{222}$ to a greater extent than it would decrease the cage fold population. As support for this view, we note that, with the exception of that of the [D9E] mutant, extrapolated $[\theta]_{F,0°C}$ values were reduced by 9−18% at pH 2.5 versus pH 7. A decrease in $[\theta]_{222}$ upon acidification is also observed (data not shown) for a

Table 2: Mutational and pH-Induced Fold Stability Changes[a]

		ΔG_U (kJ/mol)				mΔΔ*G* (kJ/mol)			ΔΔ*G*(pH) (kJ/mol)		
		∑CSDs		$\Delta G_U{}^{CD}$		NMR		CD	NMR		CD
peptide	salt bridge	280 K	300 K	300 K	T_M CD (from Figure 5)	280 K	300 K	300 K	280 K	300 K	300 K
TC10b	D−R	11.5	5.28	5.86	56						
TC10b at pH 2.5		4.64	1.93	1.89	40				(>6)	3.35	3.97
[D9E]	E−R	8.62	4.55	4.64	57	(2.9)	0.73	1.22			
[D9E] at pH 2.5		4.04	0.22	1.71	41				4.58	4.33	2.93
[D9E,R16K]	E−K	6.62	3.69	3.87	60	(4.9)	1.59	1.99			
[D9R,R16E]	R−E	6.41	3.58	3.47	56	(5.1)	1.7	2.40			
[D9R,R16E] at pH 2.5		2.32	−0.22	−0.23	25				4.1	3.80	3.7
[R16K]	D−K	5.62	2.27	3.51	54	(5.9)	3.0	2.35			
[D9E,R16O]	E−O	5.25	2.85	3.22	52	(6.25)	2.43	2.64			
[R16O][b]	D−O	4.1 ± 0.3	2.0 ± 0.2	2.71	45	(7.4)	3.3	3.16			
[R16O] at pH 2.5		2.6 ± 0.3	0.6 ± 0.2	1.12	38				1.5	1.4	1.59

[a] mΔΔ*G* is the $\Delta\Delta G_F$ associated with each mutation; positive values indicate fold destabilization. ΔΔ*G*(pH) is the effect of ionization; positive values indicate fold stabilization on deprotonation. Unless otherwise indicated, the ΔG_U values are based on the ∑CSD measure for the following shifted sites: L7 Hα, P18 Hα/Hβ3, and P19 Hδ2/δ3. With the exception of the [D9R,R16E] mutant, when G11 Hα2 shifts are available, including these larger structuring shifts, the sum does not change the ΔG_U values (±0.3 kJ/mol). [b] Because G11 Hα shifts were available throughout for this compound, an additional ∑CSD measure (the three largest structuring shifts, G11 Hα, P18Hα, and P18Hβ3) was included for evaluating ΔG_U. The average values are given.

hyperstable Trp-cage (*53*), which is >97% folded at both pH 2.5 and 7.

For species with an Asp at residue 9, the C-terminus of the helix, the helix destabilization associated with D1 protonation should be largely offset by the opposing helix stability effects associated with the C-terminal Coulombic effect on the helix: the $\Delta\Delta G_{helix}$ factors for N- and C-terminal Asp, versus alanine, measured in our laboratory are −3.7 ± 0.3 kJ/mol at pH 7 and −2.0 ± 0.2 kJ/mol at pH 2.5 for an N-terminal Asp and 2.0 ± 0.3 kJ/mol at pH 7 and 0.5 ± 0.3 kJ/mol at pH 2.5 for a C-terminal Asp (*58*). If these values apply to the Trp-cage, protonation at both D1 and D9 would disfavor the fold by only 0.2 kJ/mol because of intrinsic helicity changes; a larger effect (~1.7 kJ/mol) would be expected for any mutated sequence with Glu or Arg at residue 9. By this analysis, significant fold destabilization upon acidification for TC10b and any mutant retaining D9 implies that the Coulombic interaction between D9 and the residue 16 side chain function is stabilizing. Table 2 collects ΔG_U measures derived from chemical shifts and compares these with the values from the CD data. Table 2 includes the $m\Delta\Delta G_U$ values for each mutation and $\Delta\Delta G_U$(pH) values for those mutants examined at both pH values. The Δ*G* values are reported at both 280 and 300 K; the values at 300 K are viewed as more accurate, because these represent comparisons under conditions for which χ_F is bracketed in the 0.46−0.88 range for the mutants, where the uncertainty in the 100% and 0% folded baselines (and potential differences in CSD values associated with the mutations) will have a weaker effect on the calculations. The agreement in ΔΔ*G* measures derived from NMR and CD data is quite good; the same ranking of relative stabilities for the mutants results. Because variable levels of helicity in the unfolded state and the residual helicity of *cis*-Xxx-Pro conformers that cannot form the Trp-cage also contribute to the CD, the analysis of ring current shift measures of the cage population will be emphasized.

The $\Delta\Delta G_U$(pH) measures at 300 K will be considered first. With 0.2 and 1.7 kJ corrections for intrinsic helicity contributions for species with and without D9, respectively, the fold stabilizing contribution of the favorable Coulombic interactions between the side chains of residues 9 and 16 ranges from 1.2 to 3.8 kJ/mol, with the following ranking: D9−R16 > E9−R16 > R9−E16 > E9−O16. It is, however, difficult to judge when (if at all) this interaction shifts from being only an attractive Coulombic effect to an H-bonded salt bridge. At 280 K, all of the D9−R16, E9−R16, and R9−E16 effects are significantly larger, with the native salt bridge contribution exceeding 5 kJ/mol.

Turning to the $m\Delta\Delta G_U$ effects of a D9E mutation upon TC10b, we find this mutation is destabilizing by ~1 kJ/mol at 300 K, with a significantly larger (≥3 kJ) but less well determined amount at lower temperatures. However, when R16 is replaced with either Lys or Orn, a D9E mutation has a fold stabilizing effect (0.7−1.4 kJ/mol, whether the measurements are taken at 280 or 300 K by either CD or NMR). Because all prior mutations (N1D, L2A, I4A, and K8A) that stabilize the N-terminal helix have resulted in comparable increases in the cage fold population (*20*, *21*), stabilization of the Trp-cage fold by a D9E mutation would be expected in the absence of a salt bridge, reflecting the enhancement of the intrinsic helix formation propensity. Reflecting the salt bridge, the fold destabilizing effects of R16K and R16O mutations are significantly greater for D9 species (~3 kJ/mol) than E9 species (0.8−1.7 kJ). Specific cage-stabilizing interactions, other than salt bridges, associated with R16 are suggested by the observation that all analogues with a substitution at Arg16 are significantly destabilized [≥2 kJ/mol at 300 K (>5 kJ at 280 K)]. The NMR structure ensemble suggests that this reflects burial of the indole ring by the CH_2CH_2 unit of R16.

CONCLUSIONS

The NMR and CD studies reported here for salt bridge mutants of TC10b do not support the contention (*56*) that an E9−R16 salt bridge provides superior stabilization of the Trp cage than the D9−R16 unit that had been used in all prior cage constructs. Cage stabilizing effects, if any, of [D9E] substitutions are due to contributions from an intrinsic helicity increase and not to improvements in salt bridge formation. The helix disfavoring effect (~2 kJ/mol) of an Asp^- at the C-terminus of a helix has been recognized previously (*63*, *64*), but our study represents the first quantitation of the effect (Figure 3) and a demonstration that it has consequences in protein folding thermodynamics.

We view the absence of NMR peaks for *cis*-Xaa-Pro isomers, which are observed for all of the salt bridge mutants, for WT TC10b and the enhancement of folding cooperativity as the most compelling evidence of the greater fold stability of this species and salt bridge optimization with the D9−R16 unit. The $\Delta\Delta G$ data in Table 2 also provide evidence that (1) at 300 K, Lys and Orn substitutions at R16 are less destabilizing (0.8−1.7 kJ) for E9 species than D9 species (3−3.2 kJ), (2) the greater ΔG_U for the D9E mutant at pH 2.5 as measured by CD rather than NMR (which follows only the cage measures) suggests contributions from unfolded states that retain helicity (which would include the *cis*-Xaa-Pro species), and (3) the fold stabilizing effect of D9E when R16 is absent exists. The last of these, together with the demonstration of the destabilizing effect of the ionized side chain of D9 in model helices, suggests that it should be possible to design Trp-cage constructs that are significantly more stable under acidic conditions. Efforts in this direction are in progress.

The Trp-cage continues to provide insights into the features that stabilize both miniprotein constructs and natural proteins. The well-defined fold and reproducible chemical shift diagnostics of the Trp-cage allow access to and the interpretation of quite small (1−2 kJ/mol) stability changes. We expect that these features will continue to be a hallmark of Trp-cage studies and applications.

SUPPORTING INFORMATION AVAILABLE

Six supporting figures, including the raw CD data, thermodynamic fits, additional CD melts under acidic conditions, and the NMR evidence of *trans*-Xaa-Pro isomers of [D9E]-TC10b; details of NMR ensemble generation methods, including tables of NMR structure statistics and NOE distance constraints; and complete ^{1}H resonance assignments for [D9E]-TC10b and [D9R, R16E]-TC10b. This material is available free of charge via the Internet at http://pubs.acs.org.

REFERENCES

1. Ramírez-Alvarado, M., Blanco, F. J., and Serrano, L. (2001) Elongation of the BH8 β-hairpin peptide: Electrostatic interactions in β-hairpin formation and stability. *Protein Sci. 10*, 1381–1392.
2. Fesinmeyer, R. M., Hudson, F. M., and Andersen, N. H. (2004) Enhanced Hairpin Stability through Loop Design: The Case of the Protein G B1 Hairpin. *J. Am. Chem. Soc. 126*, 7238–7243.
3. Huyghues-Despointes, B. M., Qu, X., Tsai, J., and Scholtz, J. M. (2006) Terminal Ion Pairs Stabilize the Second β-Hairpin of the B1 Domain of Protein G. *Proteins: Struct., Funct., Bioinf. 63*, 1005–1017.
4. Rose, G. D., and Wolfenden, R. (1993) Hydrogen Bonding, Hydrophobicity, Packing, and Protein Folding. *Annu. Rev. Biophys. Biomol. Struct. 22*, 381–415.
5. Fersht, A. R., Shi, J.-P., Knill-Jones, J., Lowe, D. M., Wilkinson, A. J., Blow, D. M., Brick, P., Carter, P., Waye, M. M. Y., and Winter, G. (1985) Hydrogen bonding and biological specificity analysed by protein engineering. *Nature 314*, 235–238.
6. Fersht, A. R. (1987) The hydrogen bond in molecular recognition. *Trends Biochem. Sci. 12*, 301–304.
7. Anderson, D. E., Becktel, W. J., and Dahlquist, F. W. (1990) pH-induced denaturation of proteins: A single salt bridge contributes 3−5 kcal/mol to the free energy of folding of T4 lysozyme. *Biochemistry 29*, 2403–2408.
8. Tissot, A. C., Vuilleumier, S., and Fersht, A. R. (1996) Importance of Two Buried Salt Bridges in the Stability and Folding Pathway of Barnase. *Biochemistry 35*, 6786–6794.
9. Waldburger, C. D., Schildbach, J. F., and Sauer, R. T. (1995) Are buried salt bridges important for protein stability and conformational specificity? *Nat. Struct. Mol. Biol. 2*, 122–128.
10. Bang, D., Tereshko, V., Kossiakoff, A. A., and Kent, S. B. H. (2009) Role of a salt bridge in the model protein crambin explored by chemical protein synthesis: X-ray structure of a unique protein analogue, [V15A]crambin-α-carboxamide. *Mol. BioSyst. 5*, 750–756.
11. Dey, M., Cao, C., Sicheri, F., and Dever, T. E. (2007) Conserved Intermolecular Salt Bridge Required for Activation of Protein Kinases PKR, GCN2, and PERK. *J. Biol. Chem. 282*, 6653–6660.
12. Dong, F., and Zhou, H.-X. (2002) Electrostatic Contributions to T4 Lysozyme Stability: Solvent-Exposed Charges versus Semi-Buried Salt Bridges. *Biophys. J. 83*, 1341–1347.
13. Horovitz, A., Serrano, L., Avron, B., Bycroft, M., and Fersht, A. R. (1990) Strength and co-operativity of contributions of surface salt bridges to protein stability. *J. Mol. Biol. 216*, 1031–1044.
14. Sali, D., Bycroft, M., and Fersht, A. R. (1991) Surface electrostatic interactions contribute little to stability of barnase. *J. Mol. Biol. 220*, 779–788.
15. Makhatadze, G. I., Loladze, V. V., Ermolenko, D. N., Chen, X., and Thomas, S. T. (2003) Contribution of Surface Salt Bridges to Protein Stability: Guidelines for Protein Engineering. *J. Mol. Biol. 327*, 1135–1148.
16. Loladze, V. V., Ibarra-Molero, B., Sanxhez-Ruiz, J. M., and Makhatadze, G. I. (1999) Engineering a Thermostable Protein via Optimization of Charge-Charge Interactions on the Protein Surface. *Biochemistry 38*, 16419–16423.
17. Horng, J.-C., Moroz, V., Rigotti, D. J., Fairman, R., and Raleigh, D. P. (2002) Characterization of Large Peptide Fragments Derived from the N-Terminal Domain of the Ribosomal Protein L9: Definition of the Minimum Folding Motif and Characterization of Local Electrostatic Interactions. *Biochemistry 41*, 13360–13369.
18. Cho, J.-H., and Raleigh, D. P. (2005) Mutational analysis demonstrates that specific electrostatic interactions can play a key role in the denatured state ensemble of proteins. *J. Mol. Biol. 353*, 174–185.
19. Neidigh, J. W., Fesinmeyer, R. M., and Andersen, N. H. (2002) Designing a 20-residue protein. *Nat. Struct. Biol. 9*, 425–430.
20. Lin, J. C., Barua, B., and Andersen, N. H. (2004) The Helical Alanine Controversy: An $(Ala)_6$ Insertion Dramatically Increases Helicity. *J. Am. Chem. Soc. 126*, 13679–13684.
21. Barua, B., Lin, J. C., Williams, D. V., Neidigh, J. W., Kummler, P., and Andersen, N. H. (2008) The Trp-cage: Optimizing the Stability of a Globular Miniprotein. *Protein Eng., Des. Sel. 21*, 171–185.
22. Simmerling, C. L., Strockbine, B., and Roitberg, A. E. (2002) All-atom structure prediction and folding simulation of a stable protein. *J. Am. Chem. Soc. 124*, 11258–11259.
23. Snow, C. D., Zagrovic, B., and Pande, V. S. (2002) The Trp Cage: Folding Kinetics and Unfolded State Topology via Molecular Dynamics Simulations. *J. Am. Chem. Soc. 124*, 14548–14549.
24. Chowdhury, S., Lee, M. C., Xiong, G., and Duan, Y. (2003) *Ab initio* Folding Simulation of the Trp-cage Mini-protein Approaches NMR Resolution. *J. Mol. Biol. 327*, 711–717.
25. Pitera, J. W., and Swope, W. (2003) Understanding folding and design: Replica-exchange simulation of "Trp-cage" miniproteins. *Proc. Natl. Acad. Sci. U.S.A. 100*, 7587–7592.
26. Schug, A., Herges, T., and Wenzel, W. (2003) Reproducible Protein Folding with the Stochastic Tunneling Method. *Phys. Rev. Lett. 91*, 158102/1–158102/4.
27. Zhou, R. (2003) Trp-cage: Folding free energy landscape in explicit water. *Proc. Natl. Acad. Sci. U.S.A. 100*, 13280–13285.
28. Carnevali, P., Toth, G., Toubassi, G., and Siavash, N. (2003) Fast Protein Structure Prediction using Monte Carlo Simulations with Modal Moves. *J. Am. Chem. Soc. 125*, 14244–14245.
29. Ota, M., Ikeguchi, M., and Kidera, A. (2004) Phylogeny of protein-folding trajectories reveals a unique pathway to native structure. *Proc. Natl. Acad. Sci. U.S.A. 101*, 17658–17663.
30. Schug, A., Wenzel, W., and Hansmann, U. H. E. (2005) Energy landscape paving simulations of the trp-cage protein. *J. Chem. Phys. 122*, 194711/1–194711/7.
31. Ding, F., Buldyrev, S. V., and Dokholyan, N. V. (2005) Folding Trp-cage to NMR resolution native structure using a coarse-grained protein model. *Biophys. J. 88*, 147–155.
32. Linhananta, A., Boer, J., and MacKay, I. (2005) The equilibrium properties and folding kinetics of an all-atom Go model. *J. Chem. Phys. 122*, 114901–114915.
33. Chen, J., Im, W., and Brooks, C. L., III (2006) Balancing Solvation and Intramolecular Interactions: Toward a Consistent Generalized Born Force Field. *J. Am. Chem. Soc. 128*, 3728–3736.
34. Ulmschneider, J. P., Ulmschneider, M. B., and Di Nola, A. (2006) Monte Carlo vs Molecular Dynamics for All-Atom Polypeptide Folding Simulation. *J. Phys. Chem. B 110*, 16733–16742.
35. Juraszek, J., and Bolhuis, P. G. (2006) Sampling the multiple folding mechanisms of Trp-cage in explicit solvent. *Proc. Natl. Acad. Sci. U.S.A. 103*, 15859–15864.
36. Kentsis, A., Gindin, T., Mezei, M., and Osman, R. (2007) Calculation of the free energy and cooperativity of protein folding. *PLoS One 2*, e446.

37. Beck, D. A. C., White, G. W. N., and Daggett, V. (2007) Exploring the energy landscape of protein folding using replica-exchange and conventional molecular dynamics simulations. *J. Struct. Biol. 157*, 514–523.
38. Bendová-Biedermannová, L., Hobza, P., and Vondrášek, J. (2008) Identifying stabilizing key residues in proteins using interresidue interaction energy matrix. *Proteins: Struct., Funct., Bioinf. 72*, 402–413.
39. Hu, Z., Tang, Y., Wang, H., Zhang, X., and Lei, M. (2008) Dynamics and cooperativity of Trp-cage folding. *Arch. Biochem. Biophys. 475*, 140–147.
40. Searle, M. S., and Ciani, B. (2004) Design of β-sheet systems for understanding the thermodynamics of kinetics of protein folding. *Curr. Opin. Struct. Biol. 14*, 1–7.
41. Mok, K. H., Kuhn, L. T., Goez, M., Day, I. J., Lin, J. C., Andersen, N. H., and Hore, P. J. (2007) A pre-existing hydrophobic collapse in the unfolded state of an ultrafast folding protein. *Nature 447*, 106–109.
42. Naduthambi, D., and Zondlo, N. J. (2006) Stereoelectronic Tuning of the Structure and Stability of the Trp Cage Miniprotein. *J. Am. Chem. Soc. 128*, 12430–12431.
43. Juraszek, J., and Bolhuis, P. G. (2008) Rate Constant and Reaction Coordinate of Trp-Cage Folding in Explicit Water. *Biophys. J. 95*, 4246–4257.
44. Xu, W., and Mu, Y. (2008) Ab initio folding simulation of Trp cage by replica exchange with hybrid Hamiltonian. *Biophys. Chem. 137*, 116–125.
45. Cerný, J., Vondrásek, J., and Hobza, P. (2009) Loss of Dispersion Energy Changes the Stability and Folding/Unfolding Equilibrium of the Trp-Cage Protein. *J. Phys. Chem. B 113*, 5657–5660.
46. Marinelli, F., Pietrucci, F., Laio, A., and Piana, S. (2009) A Kinetic Model of Trp-Cage Folding from Multiple Biased Molecular Dynamics Simulations. *PLoS Comput. Biol. 5*, e1000452.
47. Bunagan, M. R., Yang, X., Saven, J. G., and Gai, F. (2006) Ultrafast Folding of a Computational Designed Trp-Cage Mutant: Trp^2-Cage. *J. Phys. Chem. B 110*, 3759–3763.
48. Chatterjee, C., and Gerig, J. T. (2006) Interactions of Hexafluoro-2-propanol with the Trp-Cage Peptide. *Biochemistry 45*, 14665–14674.
49. Chatterjee, C., and Gerig, J. T. (2007) Interactions of trifluroethanol with the Trp-cage peptide. *Biopolymers 87*, 115–123.
50. Neuman, R. C., and Gerig, J. T. (2008) Solvent interactions with the Trp-cage peptide in 35% ethanol−water. *Biopolymers 89*, 862–872.
51. Wafer, L. N. R., Streicher, W. W., and Makhatadze, G. I. (2010) Thermodynamics of the Trp-cage miniprotein unfolding in urea. *Proteins: Struct., Funct., Bioinf. 78*, 1376–1381.
52. Andersen, N. H., Barua, B., Fesinmeyer, R. M., Hudson, F. M., Lin, J., Euser, A., and White, G. (2002) in Peptides 2002: Proceedings of the 27th European Peptide Symposium, pp 824−825, Edizioni Ziino, Napoli, Italy.
53. Williams, D. V., Barua, B., and Andersen, N. H. (2008) A Hyperstable Miniprotein: Additive Effects of D- and L-Ala Substitutions. *Org. Biomol. Chem. 6*, 4287–4289.
54. Streicher, W. W., and Makhatadze, G. I. (2007) Unfolding Thermodynamics of Trp-Cage, a 20 Residue Miniprotein, Studied by Differential Scanning Calorimetry and Circular Dichroism Spectroscopy. *Biochemistry 46*, 2876–2880.
55. Day, R., Paschek, D., and Garcia, A. E. (2010) Microsecond simulations of the folding/unfolding thermodynamics of the Trp-cage miniprotein. *Proteins: Struct., Funct., Bioinf. 78*, 1889–1899.
56. Hudaky, P., Straner, P., Farkas, V., Varadi, G., Toth, G., and Perczel, A. (2008) Cooperation between a Salt Bridge and the Hydrophobic Core Triggers Fold Stabilization in a Trp-Cage Miniprotein. *Biochemistry 47*, 1007–1016.
57. Barua, B. (2005) Design and Study of Trp-cage Miniproteins. Ph.D. Thesis, University of Washington, Seattle.
58. Stewart, J. M. (2009) The use of ^{13}C Carbonyl labeled Residues to Develop and Refine Site-Specific NMR Secondary Structure Analysis Techniques. Ph.D. Thesis, University of Washington, Seattle.
59. Andersen, N. H., and Tong, H. (1997) Empirical parameterization of a model for predicting peptide helix/coil equilibrium populations. *Protein Sci. 6*, 1920–1936.
60. Song, K., Stewart, J. M., Fesinmeyer, R. M., Andersen, N. H., and Simmerling, C. (2008) Structural insights for designed alanine-rich helices: Comparing NMR helicity measures and conformational ensembles from molecular dynamics simulation. *Biopolymers 89*, 747–760.
61. Stewart, J. M., Lin, J. C., and Andersen, N. H. (2008) Lysine and arginine residues do not increase the helicity of alanine-rich helices. *Chem. Commun.*, 4765–4767.
62. Fesinmeyer, R. M. (2005) Chemical Shifts Define the Structure and Folding Thermodynamics of Polypeptides. Ph.D. Thesis, University of Washington, Seattle.
63. Doig, A. J., and Baldwin, R. L. (1995) N- and C-capping preferences for all 20 amino acids in α-helical peptides. *Protein Sci. 4*, 1325–1336.
64. Huyghues-Despointes, B. M., Scholtz, J. M., and Baldwin, R. L. (1993) Effect of a single aspartate on helix stability at different positions in a neutral alanine-based peptide. *Protein Sci. 2*, 1604–1611.